

Real-time evolution method and its application to 3α cluster system

R. Imai and T. Tada

Department of Physics, Hokkaido University, 060-0810 Sapporo, Japan

M. Kimura*

Department of Physics, Hokkaido University, 060-0810 Sapporo, Japan and

*Nuclear Reaction Data Centre, Faculty of Science,
Hokkaido University, 060-0810 Sapporo, Japan*

(Dated: March 3, 2022)

Abstract

A new theoretical method is proposed to describe the ground and excited cluster states of atomic nuclei. The method utilizes the equation-of-motion of the Gaussian wave packets to generate the basis wave functions having various cluster configurations. The generated basis wave functions are superposed to diagonalize the Hamiltonian. In other words, this method uses the real time as the generator coordinate. The application to the 3α system as a benchmark shows that the new method works efficiently and yields the result consistent with or better than the other cluster models. Brief discussion on the structure of the excited 0^+ and 1^- states is also made.

* masaaki@nucl.sci.hokudai.ac.jp

I. INTRODUCTION

It has long been known that the Hoyle state (the 0_2^+ state of ^{12}C) is a dilute gas-like α cluster state dominated by the s -wave [1–8]. Later, it was pointed out that the Hoyle state can be regarded as a Bose-Einstein condensate of α particles [9–11]. This findings motivated many studies on ^{12}C and the related topics. For example, the idea of the α particle condensate has been extended to other excited states above the Hoyle state. Namely, the 2^+ state at 10.03 MeV [12–15] and the 4^+ state at 13.3 MeV [16] are considered as the members of the "Hoyle band" [11, 17, 18]. More recently, the 0_3^+ state at 10.3 MeV [13, 19] is suggested as the "breathing mode" of the Hoyle state [18, 20–24]. The possible formation of the 3α linear-chain (0_4^+ state) has also been discussed [18, 23].

The discussion has been naturally extended to the condensate of many α particles. The candidates of the 4α condensate in ^{16}O are under the intensive discussions [25–32]. However, the theoretical and experimental information for the 5α and more α particle condensate [11, 33–35] is rather scarce. The clustering of non- α nuclei is another direction of the extension. For example, the Hoyle-analog states with a nucleon hole or particle are discussed for ^{11}B [36–39] and ^{13}C [40, 41]. The 3α linear-chains accompanied by the valence neutrons are expected in neutron-rich C isotopes [42–53]. Thus, nowadays the researches are extending to the highly excited cluster states composed of many clusters and nucleons.

However, when the number of the constituent clusters or nucleons increases, the description of the cluster states becomes difficult. For example, suppose that one employs the generator coordinate method (GCM) [54, 55] which superposes many basis wave functions. Then, it is easy to imagine that the number of basis wave functions required for the description of the cluster states increases very quickly as the number of constituent particles increases or the system becomes dilute. As a result, much computational power is demanded and the practical calculation becomes difficult. This may be one of the reason why the 5α and more α particle condensate are rarely studied based on the microscopic models. Therefore, new method which efficiently generates the basis wave functions is highly desirable and indispensable. For this purpose, several methods have been developed such as the stochastic sampling of the basis wave functions [56–58] and the imaginary-time development method [59].

In this study, we propose an alternative method which utilizes the equation-of-motion

(EOM) of the Gaussian wave packets. The basis wave functions are generated by the real-time evolution of the system governed by the EOM, and they are superposed to diagonalize the Hamiltonian. In other words, this method employs the real time as the generator coordinate. As a benchmark of the methodology, we applied it to the 3α system (^{12}C). It is shown that the new method works efficiently and yields the result consistent with or better than the other cluster models. Furthermore, based on the isoscalar (IS) monopole and dipole transition strengths, we briefly discuss the structure of the excited 0^+ and 1^- states.

This paper is organized as follows. In the next section, we explain the framework of the new method named real-time evolution method (REM). In the section III, we present the result of the numerical benchmark. We also discuss the structure of the excited 0^+ and 1^- states briefly. The final section summarizes this work.

II. THEORETICAL FRAMEWORK

Here, we explain the framework of the real-time evolution method. For simplicity, we assume its application to the α cluster wave functions ($4N$ nuclei). However, it is noted that the method is also applicable to more general cases such as non- α cluster wave functions, antisymmetrized molecular dynamics (AMD) and fermionic molecular dynamics (FMD) wave functions.

A. Hamiltonian and GCM wave function

The Hamiltonian for the $N\alpha$ systems composed of $4N$ nucleons is given as,

$$\hat{H} = \sum_{i=1}^{4N} \hat{t}_i + \sum_{i<j}^{4N} \hat{v}_N(r_{ij}) + \sum_{i<j}^{4N} \hat{v}_C(r_{ij}) - \hat{t}_{cm}, \quad (1)$$

where \hat{t}_i and \hat{t}_{cm} respectively denote the kinetic energies of the nucleons and the center-of-mass. The \hat{v}_N and \hat{v}_C denote the effective nucleon-nucleon interaction and Coulomb interactions, respectively. The parameter set of \hat{v}_N is explained later.

As for the intrinsic wave function of $N\alpha$ system, we employ the Brink-Bloch wave function

[60] which is composed of α clusters having $(0s)^4$ configurations,

$$\Phi(\mathbf{Z}_1, \dots, \mathbf{Z}_N) = \mathcal{A} \{ \Phi_\alpha(\mathbf{Z}_1) \cdots \Phi_\alpha(\mathbf{Z}_N) \}, \quad (2)$$

$$\Phi_\alpha(\mathbf{Z}) = \mathcal{A} \{ \phi(\mathbf{r}_1, \mathbf{Z}) \chi_{p\uparrow} \cdots \phi(\mathbf{r}_4, \mathbf{Z}) \chi_{n\downarrow} \}, \quad (3)$$

$$\phi(\mathbf{r}, \mathbf{Z}) = \left(\frac{2\nu}{\pi} \right)^{3/4} \exp \left\{ -\nu \left(\mathbf{r} - \frac{\mathbf{Z}}{\sqrt{\nu}} \right)^2 + \frac{1}{2} Z^2 \right\}. \quad (4)$$

Here $\Phi_\alpha(\mathbf{Z})$ denotes the wave packet describing the α cluster located at \mathbf{Z} . The three-dimensional vectors $\mathbf{Z}_1, \dots, \mathbf{Z}_N$ are complex numbered and describe the α cluster positions in the phase space.

Similarly to other cluster models, we superpose the intrinsic wave function having different configurations (different sets of the complex vectors $\mathbf{Z}_1, \dots, \mathbf{Z}_N$) after the parity and angular momentum projection (GCM). The most general form of the GCM wave function may be written as,

$$\begin{aligned} \Psi_M^{J\pi} &= \sum_K \int d^3 Z_1 \dots d^3 Z_N \\ &\times f_K(\mathbf{Z}_1, \dots, \mathbf{Z}_N) \hat{P}_{MK}^{J\pi} \Phi(\mathbf{Z}_1, \dots, \mathbf{Z}_N), \end{aligned} \quad (5)$$

where $\hat{P}_{MK}^{J\pi}$ is the parity and angular momentum projector. The amplitude of the superposition $f_K(\mathbf{Z}_1, \dots, \mathbf{Z}_N)$ must be determined in some ways. For example, the original THSR wave function ($J = M = K = 0$) [9] asserts that the amplitude can be written as

$$f_0(\mathbf{R}_1, \dots, \mathbf{R}_N) = \prod_{i=1}^N \exp \left\{ -\frac{1}{2\beta^2} R_i^2 \right\}, \quad (6)$$

where the vectors $\mathbf{Z}_1, \dots, \mathbf{Z}_N$ are reduced to the real valued vectors $\mathbf{R}_1, \dots, \mathbf{R}_N$, and the parameter β controls the size of the α particle condensate. It is known that this THSR ansatz works surprisingly well for the ground and excited 0^+ states of ^{12}C [9–11, 61].

In other ordinary cluster models, Eq. (5) is often discretized and approximated by a sum of the finite number of the basis wave functions,

$$\Psi_M^{J\pi} = \sum_{p=1}^{p_{max}} \sum_{K=-J}^J f_{pK} \hat{P}_{MK}^{J\pi} \Phi(\mathbf{Z}_1^{(p)}, \dots, \mathbf{Z}_N^{(p)}), \quad (7)$$

and the amplitude f_{pK} is calculated by the Griffin-Hill-Wheeler equation [54, 55]. Here, $\mathbf{Z}_1^{(p)}, \dots, \mathbf{Z}_N^{(p)}$ denotes the p th set of the vectors $\mathbf{Z}_1, \dots, \mathbf{Z}_N$ and the number of the superposed basis wave function is equal to p_{max} . If p_{max} is sufficiently large and the set of the vectors

$\mathbf{Z}_1^{(p)}, \dots, \mathbf{Z}_N^{(p)}$ covers various configurations of α clusters, Eq. (7) will be a good approximation, but the increase of p_{max} requires much computational cost. It is easy to imagine that the number of basis wave function p_{max} required for a reasonable description of $N\alpha$ systems will be greatly increased, when the number of α particle is increased. This is one of the reason, for example, why the condensation of 5 and more α particles are rarely studied by the microscopic models.

Therefore, if one employs the approximation given by Eq. (7), it is essentially important to find a method which *efficiently* generates the set of the vectors $\mathbf{Z}_1^{(p)}, \dots, \mathbf{Z}_N^{(p)}$ to reduce the computational cost. For this purpose, several methods such as the stochastic method [56–58] and the imaginary time evolution methods [59] have been proposed, and in this study, we introduce a new method which uses the real-time evolution of the α particle wave packets.

B. Real-time evolution method

In the present study, the EOM of the α particle wave packets is used to generate the sets of the vectors $\mathbf{Z}_1^{(p)}, \dots, \mathbf{Z}_N^{(p)}$. By applying the time-dependent variational principle to the intrinsic wave function given by Eq. (2),

$$\delta \int dt \frac{\langle \Phi(\mathbf{Z}_1, \dots, \mathbf{Z}_N) | i\hbar d/dt - \hat{H} | \Phi(\mathbf{Z}_1, \dots, \mathbf{Z}_N) \rangle}{\langle \Phi(\mathbf{Z}_1, \dots, \mathbf{Z}_N) | \Phi(\mathbf{Z}_1, \dots, \mathbf{Z}_N) \rangle} = 0, \quad (8)$$

one obtains the EOM for the α particle centroids $\mathbf{Z}_1, \dots, \mathbf{Z}_N$,

$$i\hbar \sum_{j=1}^N \sum_{\sigma=x,y,z} C_{i\rho j\sigma} \frac{dZ_{j\sigma}}{dt} = \frac{\partial \mathcal{H}_{int}}{\partial Z_{i\rho}^*}, \quad (9)$$

$$\mathcal{H}_{int} \equiv \frac{\langle \Phi(\mathbf{Z}_1, \dots, \mathbf{Z}_N) | \hat{H} | \Phi(\mathbf{Z}_1, \dots, \mathbf{Z}_N) \rangle}{\langle \Phi(\mathbf{Z}_1, \dots, \mathbf{Z}_N) | \Phi(\mathbf{Z}_1, \dots, \mathbf{Z}_N) \rangle}, \quad (10)$$

$$C_{i\rho j\sigma} \equiv \frac{\partial^2 \ln \langle \Phi(\mathbf{Z}_1, \dots, \mathbf{Z}_N) | \Phi(\mathbf{Z}_1, \dots, \mathbf{Z}_N) \rangle}{\partial Z_{i\rho}^* \partial Z_{j\sigma}}. \quad (11)$$

Starting from an arbitrary initial wave function at $t = 0$, we solve the time evolution of $\mathbf{Z}_1, \dots, \mathbf{Z}_N$. As a result, the EOS yields the set of the vectors $\mathbf{Z}_1(t), \dots, \mathbf{Z}_N(t)$ as function of the time t , which defines the wave function $\Phi(\mathbf{Z}_1(t), \dots, \mathbf{Z}_N(t))$ at each time. Despite of its classical form, this EOM still holds the information of the quantum system. For example, it was shown that the nuclear phase shift of the α - α scattering can be obtained from the classical trajectory of the wave packet centroids [62]. In addition to this, it was shown that

the ensemble of the wave functions $\Phi(\mathbf{Z}_1(t), \dots, \mathbf{Z}_N(t))$ possesses following good properties [63–65].

1. The ensemble of the time-dependent wave functions $\Phi(\mathbf{Z}_1(t), \dots, \mathbf{Z}_N(t))$ has ergodic nature
2. And it follows the *quantum* statistics

if the nucleon-nucleon collisions and nucleon emission processes are properly treated. Indeed, on the basis of this EOM properties, the nuclear liquid-gas phase transition during the heavy-ion collisions and the caloric curve for the finite nuclei have been studied [66–69]. Therefore, we expect that, if time is evolved long enough, the ensemble of the wave functions $\Phi(\mathbf{Z}_1(t), \dots, \mathbf{Z}_N(t))$ spans a good model space for $N\alpha$ systems. In other words, we expect that the bound and resonant states of $N\alpha$ systems are reasonably described by the superposition of the basis wave functions as follows,

$$\Psi_M^{J\pi}(T) = \int_0^T dt \sum_{K=-J}^J \hat{P}_{MK}^{J\pi} \left\{ f_K(t) \Phi(\mathbf{Z}_1(t), \dots, \mathbf{Z}_N(t)) + g_K(t) \Phi(\mathbf{Z}_1^*(t), \dots, \mathbf{Z}_N^*(t)) \right\}. \quad (12)$$

Here, the complex conjugated basis wave functions are also superposed to properly describe time-even states. The coefficients $f_K(t)$ and $g_K(t)$ should be determined by the diagonalization of the Hamiltonian. Eq. (12) can be regarded as the GCM wave function which employs the real-time t as the generator coordinate.

C. Numerical calculation

In this study, REM calculation is performed for 3α cluster system (^{12}C). For the sake of the comparison, we used the Volkov No. 2 effective nucleon-nucleon interaction [70] with a slight modification [2, 3], which is common to the other studies using resonating group method (RGM) [2, 3] and Tohsaki-Horiuchi-Schuck-Röpke (THSR) wave function [18, 23, 61]. The numerical calculation was performed in the following steps.

- (1) In the first step, we randomly generate 3α cluster wave function and calculate the *imaginary-time* evolution of the system,

$$i\hbar \frac{d\mathbf{Z}_i}{d\tau} = \mu \frac{\partial \mathcal{H}_{int}}{\partial \mathbf{Z}_i^*}, \quad (13)$$

where μ is an arbitrary negative number. Eq. (13) decreases the intrinsic energy \mathcal{H}_{int} , as the imaginary time τ is evolved. The imaginary-time evolution is continued until the intrinsic excitation energy,

$$E_{int}^* = \mathcal{H}_{int} - \mathcal{H}_{int}^{min}, \quad (14)$$

equals to a certain value. Here, \mathcal{H}_{int}^{min} is the minimum intrinsic energy obtained by the very long imaginary-time evolution, which is -74.5 MeV in the present Hamiltonian. In the practical calculation, we tested several values of E_{int}^* (10, 20, 25 and 30 MeV) and found that $E_{int}^* = 25$ MeV results in the best convergence.

(2) In the second step, we calculate the *real-time* evolution (Eq. (9)) starting from the initial wave function obtained in the first step. For the numerical calculation, the time is discretized with an interval of $\Delta t = 0.02$ fm/c,

$$t_p = (p - 1)\Delta t, \quad p = 1, 2, \dots, p_{max}, \quad (15)$$

and the maximal propagation time is $T_{max} = (p_{max} - 1)\Delta t = 6,000$ fm/c. It is noted that the intrinsic energy \mathcal{H}_{int} , and hence E_{int}^* , is conserved by the EOM. As a result, the time evolution calculation yields a set of the Brink-Bloch wave functions $\Phi(\mathbf{Z}_1(t_p), \dots, \mathbf{Z}_N(t_p))$, $p = 1, \dots, p_{max}$ having the same E_{int}^* . And it is used as the basis wave function of the GCM calculation in the next step.

If E_{int}^* is large, α clusters occasionally escape out to infinite distance during the time evolution. This yields basis wave functions having unphysically large radius, which are useless for the description of the bound or resonant states. To avoid this problem, we impose additional condition to the calculation. When the condition,

$$\max_i \Re(|\mathbf{Z}_i(t)|/\sqrt{\nu}) > R_{max}, \quad (16)$$

is satisfied, *i.e.* if any of α clusters is distant more than R_{max} , we interchange their momentum by hand as follows,

$$\mathbf{Z}_i(t + \Delta t) = \text{Re}(\mathbf{Z}_i(t)) - i\text{Im}(\mathbf{Z}_i(t)), \quad (17)$$

$$\mathbf{Z}_j(t + \Delta t) = \text{Re}(\mathbf{Z}_j(t)) - i\text{Im}(\mathbf{Z}_k(t)), \quad (18)$$

$$\mathbf{Z}_k(t + \Delta t) = \text{Re}(\mathbf{Z}_k(t)) - i\text{Im}(\mathbf{Z}_j(t)), \quad (19)$$

where we assume that $|\mathbf{Z}_i(t)| > R_{max}$. It is noted that the real part of $\mathbf{Z}(t)$ corresponds the coordinate of α cluster, while the imaginary part corresponds to the momentum. As a result, α clusters rebound as illustrated in Fig. 1. In the present calculation, the maximum distance is chosen as $R_{max} = 10.0$ fm.

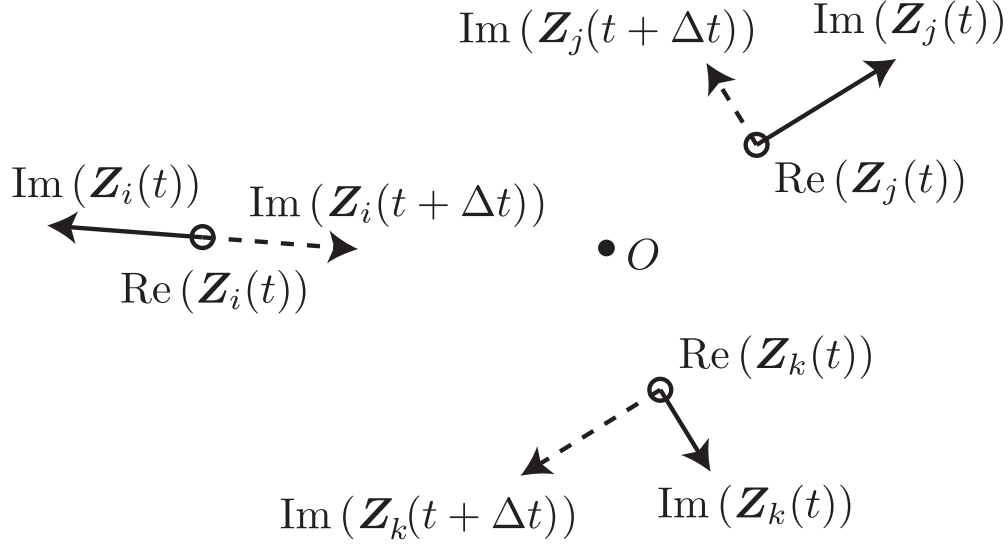


FIG. 1. The rebound of α clusters described by Eq. (17)-(19). Open circles represent the real-part of \mathbf{Z} , and the solid (dotted) arrows represent the imaginary part of \mathbf{Z} before (after) the rebound. The rebound does not change the real-parts of \mathbf{Z}_i , \mathbf{Z}_j and \mathbf{Z}_k (positions of α clusters), but changes the imaginary-parts (momenta). It reverts the momentum of \mathbf{Z}_i and the center-of-mass momentum between \mathbf{Z}_j and \mathbf{Z}_k , but conserves the relative momentum between \mathbf{Z}_j and \mathbf{Z}_k .

(3) Thus-obtained basis wave functions are superposed by using the real-time t as a generator coordinate. In the following we call this step GCM calculation. Since the time is discretized, Eq. (12) should read,

$$\Psi_M^{J\pi} = \sum_{p=1}^{p_{max}} \sum_{K=-J}^J \hat{P}_{MK}^{J\pi} \left\{ f_K(t_p) \Phi(t_p) + g_K(t_p) \Phi^*(t_p) \right\}, \quad (20)$$

Here, the basis wave function $\Phi(\mathbf{Z}_1(t_p), \dots, \mathbf{Z}_N(t_p))$ is abbreviated as $\Phi(t_p)$. The set of the coefficient $f_K(t_p)$, $g_K(t_p)$ and the eigen-energy are determined by solving the Griffin-Hill-Wheeler equation to diagonalize the Hamiltonian.

In the practical calculation, a set of basis wave functions $\Phi(t_p)$ obtained by the time evolution is severely redundant. This makes it difficult to solve the Griffin-Hill-Wheeler

equation accurately. To avoid this problem, we remove the basis wave functions which have large overlap with others. When a basis wave function $\Phi(t_p)$ satisfies the following condition,

$$\max_{t < t_p} \frac{|\langle \Phi(t) | \Phi(t_p) \rangle|^2}{\langle \Phi(t) | \Phi(t) \rangle \langle \Phi(t_p) | \Phi(t_p) \rangle} > O_{max}, \quad (21)$$

it is removed from the ensemble. Namely, we do not use the basis wave functions which have the overlap with the past wave functions larger than O_{max} . In the present calculation O_{max} is chosen as 0.75.

(4) As discussed later, above-explained GCM calculation has problem to describe highly excited broad resonances, because of contamination of the non-resonant wave functions. To overcome this problem, we apply the r^2 -constraint method proposed by Funaki *et al.* [71]. Following this method, we first diagonalize the radius operator,

$$\sum_{K'q} \langle \hat{P}_{MK}^{J\pi} \Phi(t_p) | \hat{r}^2 - r_a^2 | \hat{P}_{MK'}^{J\pi} \Phi(t_q) \rangle e_{K'qa} = 0, \quad (22)$$

$$\hat{r}^2 = \sum_{i=1}^{4N} (\mathbf{r}_i - \mathbf{r}_{cm})^2 / (4N), \quad (23)$$

which defines a new set of the basis wave functions,

$$\tilde{\Phi}_{Ma}^{J\pi} = \sum_{Kp} e_{Kpa} P_{MK}^{J\pi} \Phi(t_p), \quad (24)$$

corresponding to the eigenvalue r_a^2 . Superposing these new basis, we construct the r^2 -constrained GCM wave function,

$$\Psi_M^{J\pi} = \sum'_{a(r_a^2 < r_{cut}^2)} \left\{ \tilde{f}_a \tilde{\Phi}_{Ma}^{J\pi} + \tilde{g}_a \tilde{\Phi}_{Ma}^{J\pi*} \right\}. \quad (25)$$

Here \sum' denotes the conditional summation running over all a which satisfy the condition $r_a^2 < r_{cut}^2$. Namely, the basis wave functions which have too large eigenvalue of the radius operator are excluded. The coefficients \tilde{f}_a , \tilde{g}_a and the eigen-energies are determined by solving the Griffin-Hill-Wheeler equation. It has been shown that this method effectively separates the resonant states from the non-resonant states. In the present calculation, the cut-off radius r_{cut}^2 is varied ranging from $(5.0 \text{ fm})^2$ to $(7.0 \text{ fm})^2$ to check the convergence.

III. NUMERICAL RESULTS

In this section, we explain how our method works, and compare the obtained result with those of other models to check the validity and efficiency of the REM. The detailed discussion

on the structures of cluster states in ^{12}C will be made in our forthcoming work.

A. Real-time evolution

As explained in the previous section, the REM relies on the ergodic nature of the EOM. Therefore, if the time is propagated long enough, the results should be converged and should not depend on the initial wave functions. To check these points, we tested two different initial wave functions with $E_{int}^* = 25$ MeV to yield ensembles of the wave functions, which we denote set 1 and 2.

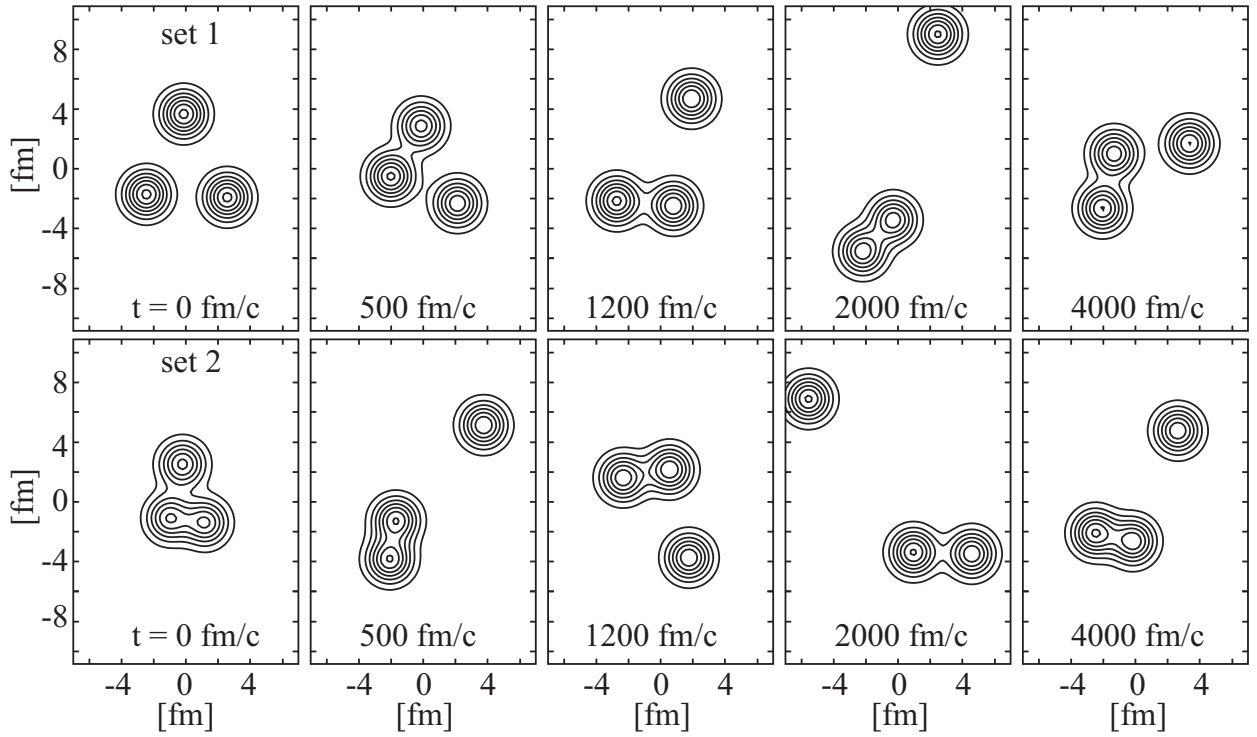


FIG. 2. Intrinsic density snapshots at the propagation time $t = 0, 500, 1200, 2000$ and 4000 fm/c. Upper (lower) panels show the ensemble of the wave functions obtained by the EOM starting from the wave function at $t = 0$ fm/c.

To illustrate how the 3α system is evolved by the EOM, Fig. 2 shows the several wave functions of set 1 and 2 at particular times. In both ensembles, disregard to the initial condition, α clusters distribute in various ways; they are close to each other in some time and far distant in another time. Actually, the system repeats spatial expansion and contraction as time being evolved, which can be confirmed from the radius of the system as function of

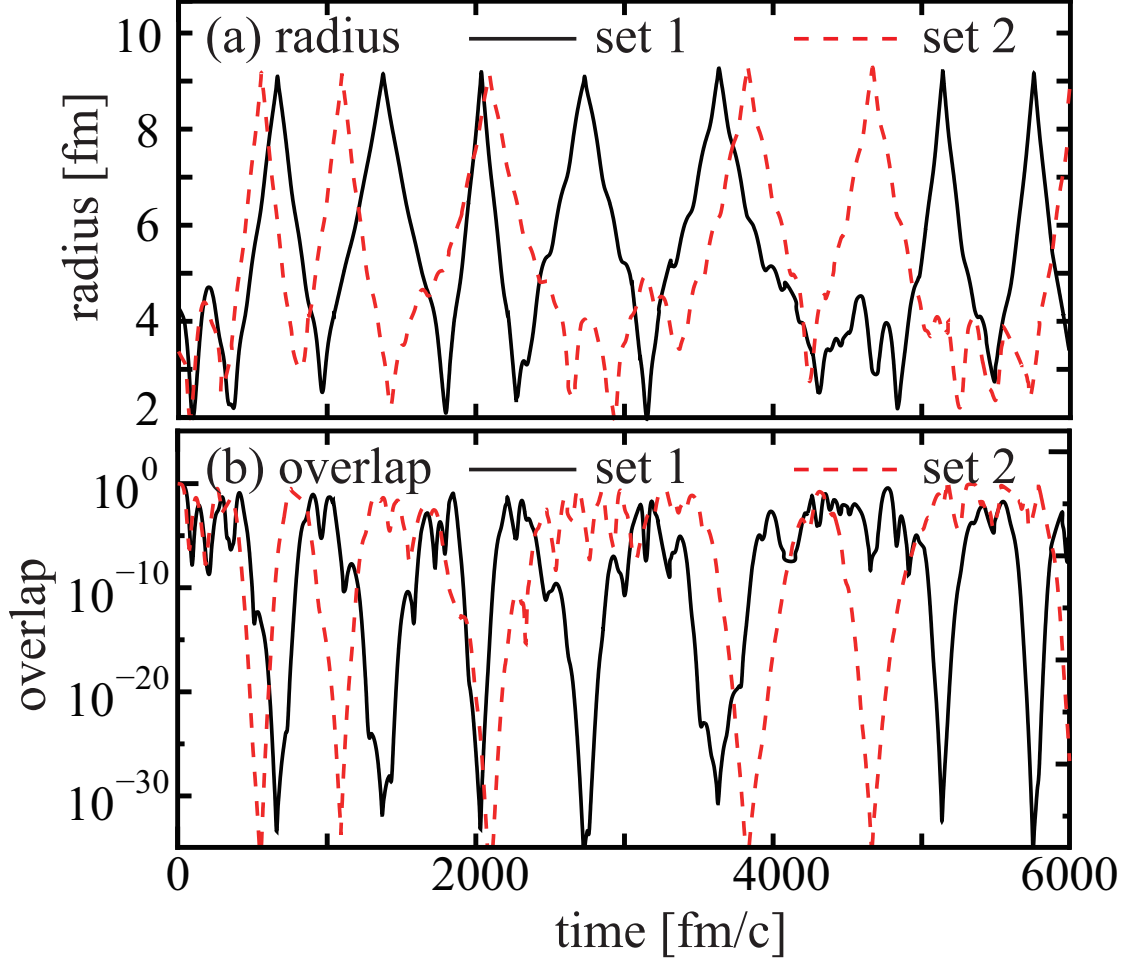


FIG. 3. (a) Radius of the intrinsic wave function as function of time. (b) Overlap between the wave functions at $t = 0$ and t after the projection to the $J^\pi = 0^+$.

time shown in Fig. 3 (a). It is noted that the unphysical change of the expansion velocity at the maximum radius around 9 fm is because of the artificial rebound of the α clusters described by Eqs. (17)-(19). Figure 3 (b) shows the squared overlap between the wave function $\Phi(t)$ and initial wave function $\Phi(0)$ after the projection to $J^\pi = 0^+$ state, that is defined as,

$$\mathcal{O}(t) = \frac{|\langle \hat{P}^{0+} \Phi(0) | \hat{P}^{0+} \Phi(t) \rangle|^2}{\langle \hat{P}^{0+} \Phi(0) | \hat{P}^{0+} \Phi(0) \rangle \langle \hat{P}^{0+} \Phi(t) | \hat{P}^{0+} \Phi(t) \rangle}. \quad (26)$$

We see that the overlap is rather small, and hence, the wave function is almost orthogonal to the initial wave function in most of the time. Thus, the EOM generates various α cluster configurations automatically.

B. Convergence without and with r^2 -constraint

We first discuss the GCM results obtained without r^2 -constraint. Figure 4 shows the energies of the 0^+ states as functions of the maximum propagation time T_{max} . We see that

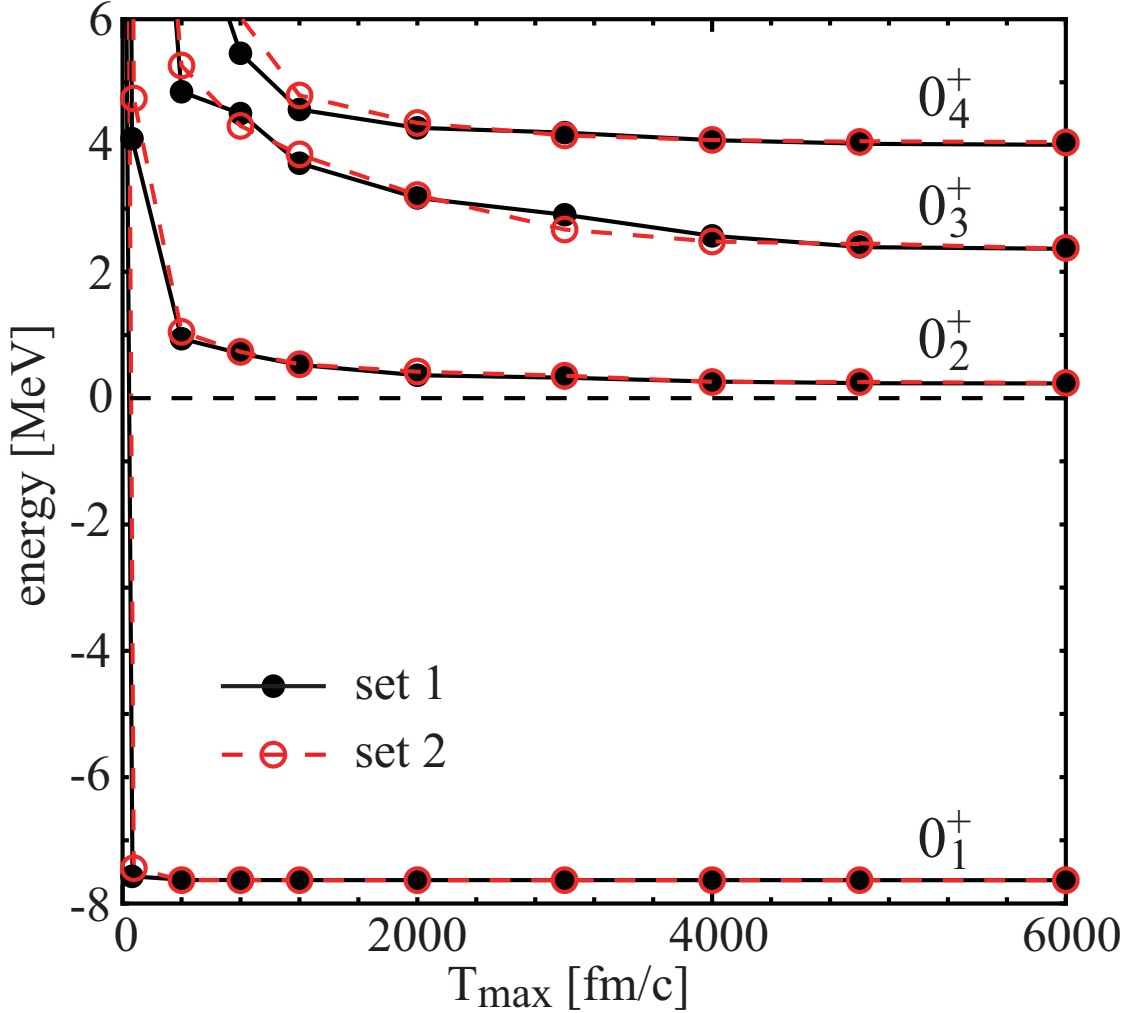


FIG. 4. (Color online) The eigen-energies of the 0^+ states measured from the 3α threshold as function of the propagation time T obtained by the REM without the r^2 -constraint. Open and filled symbols show the results obtained by using the different initial wave functions at $t = 0$ fm/c.

the energies of the 0^+ states converge and are independent of the initial wave functions, if the propagation time is long enough. In particular, the energy of the ground state converges very quickly, despite of the rather high intrinsic excitation energy ($E_{int}^* = 25$ MeV) of the basis wave functions generated by the EOM. We also found that the quick convergence is common to another bound state (2_1^+ state).

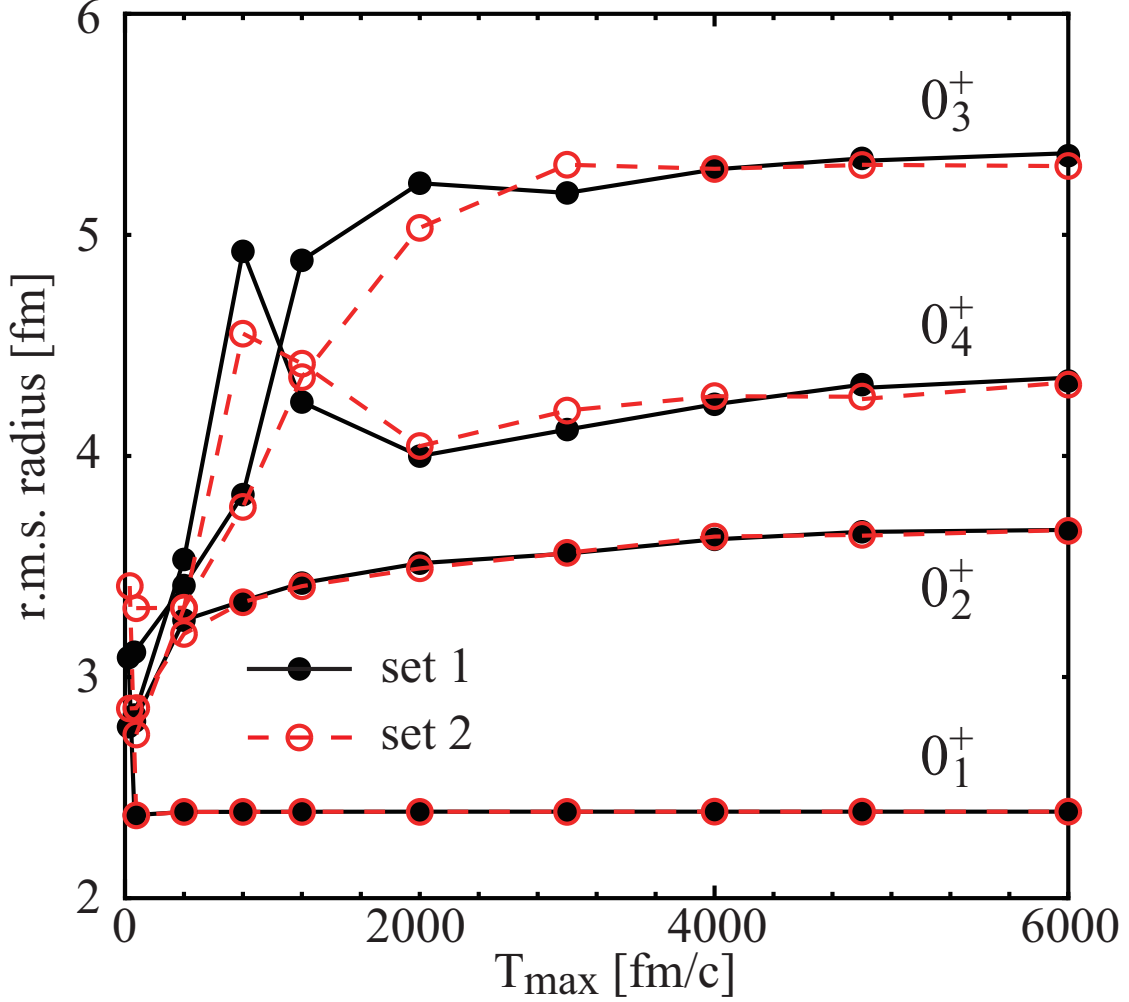


FIG. 5. (Color online) Same with Fig. 4 but for radii.

On the other hand, the energy convergence of the excited 0^+ states is not as fast as that of the ground state. In particular, it is interesting to note that the convergence of the 0_3^+ state looks much slower than others. This is related to the fact that the 0_3^+ state is a very broad resonance [13, 19]. Furthermore, if we observe the figure carefully, we find that the energies of these unbound states still go down even at large T_{max} . This is because of the contamination of the non-resonant wave functions to these excited 0^+ states, which can be seen more clearly in the T_{max} dependence of the radius shown in Fig. 5. Again we see that the convergence of the ground state is surprisingly fast, but the unbound states are not. In this figure, we clearly observe that the radii of the unbound states continuously increases showing the contamination of non-resonant wave functions with huge radii.

To avoid the contamination of the non-resonant wave functions, we applied the r^2 -constraint [71]. This prescription excludes the basis wave function with huge radius and makes it possible to obtain approximate energies and wave functions of the resonant states. Since the r^2 -constraint was already applied to THSR wave function [18, 24], it is worthwhile to compare the results between THSR and REM with r^2 -constraint. Figure 6 shows the

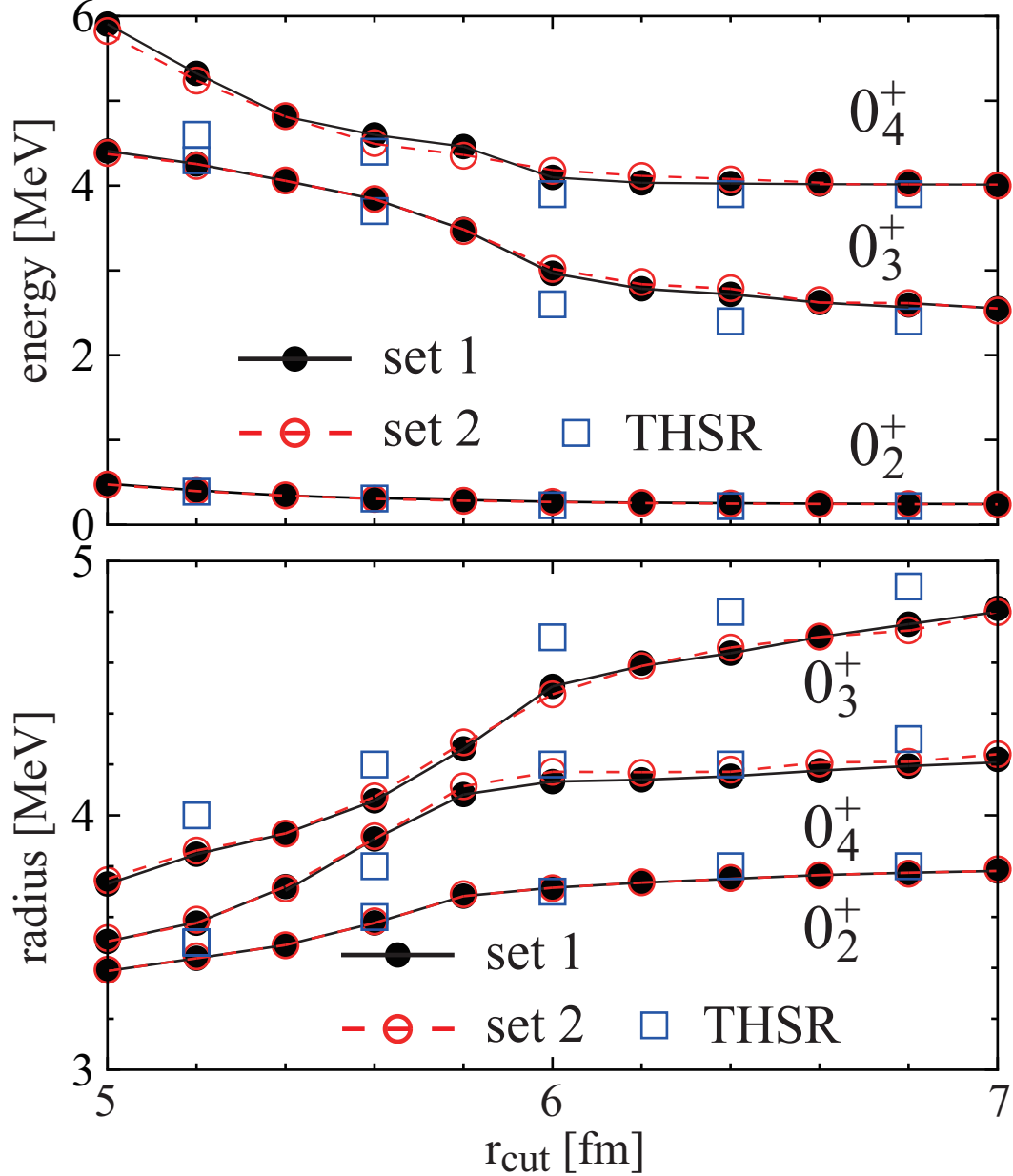


FIG. 6. (Color online) energy (upper panel) and radius (lower panel) of the excited 0^+ states obtained by the r^2 -constraint. THSR results are taken from Ref. [18]

energies and radii of the excited 0^+ states obtained by the r^2 -constraint. The energies of the 0_2^+ and 0_4^+ states are approximately constant in the region of the $r_{cut} \geq 6$ fm, and the radii are very slowly increases as function of r_{cut} . This implies that the most of the resonant wave functions in the interaction region is already described by the basis wave functions with $r_{cut} < 6$ fm, and the choice of the $6 \leq r_{cut} \leq 7$ fm will give reasonable approximation for the 0_2^+ and 0_4^+ states. We also note the results for the 0_2^+ and 0_4^+ look almost consistent with the THSR results. On the other hand, we have not obtained the reasonable convergence for the 0_4^+ state. In particular, the radius continues to increase as function of r_{cut} not only in the REM calculation but also in the THSR calculation, which implies the contamination non-resonant wave functions. This requires more sophisticated method such as the complex scaling for more precise discussion of this state [20–22].

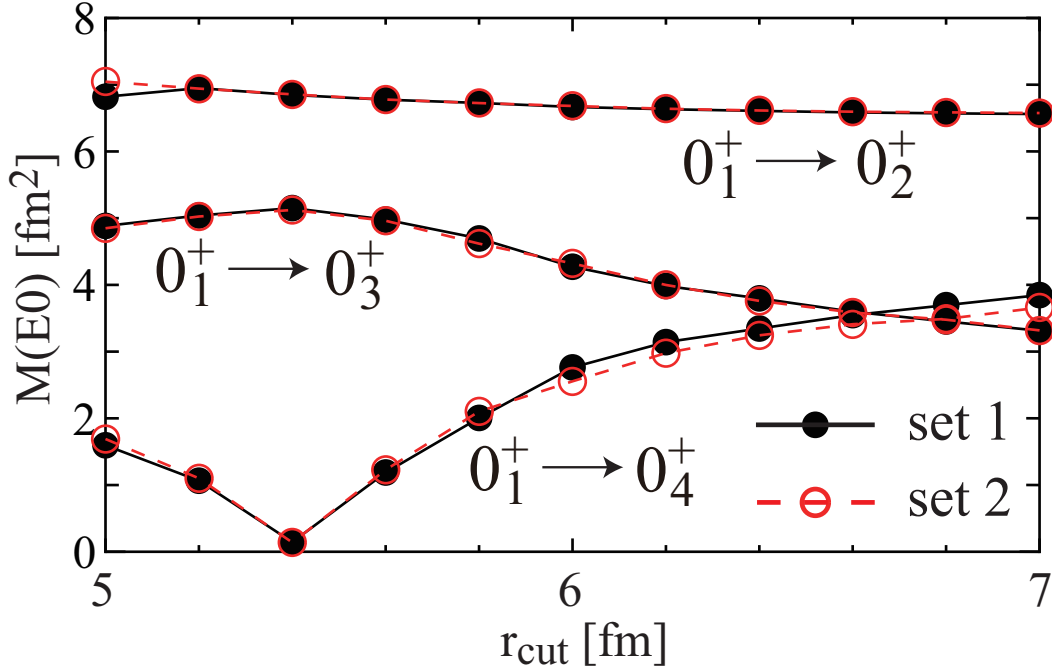


FIG. 7. (Color online) Electric monopole transition matrix from the ground state to the excited 0^+ states obtained by the r^2 -constraint.

Finally, Fig. 7 shows the electric monopole transition matrix between the ground and excited 0^+ states. Again we see that the Hoyle state is quite stable, while the 0_3^+ and 0_4^+ are dependent on r_{cut} . Since the monopole matrix element is very sensitive to the outer side of the wave functions, this behavior also indicates the non-negligible contamination of the

continuum states with large radii.

C. Excitation spectrum of ^{12}C

Here, we discuss the excitation spectrum of ^{12}C and make brief comments on the structure of several states. Figure 8 shows the excitation spectrum of ^{12}C calculated by the REM with the ensemble set 1 and $r_{cut} = 6.4$ fm together with those by the RGM [2, 3] and THSR [18, 23]. Their energies and radii are also listed in Tab. I. Note that all of these calculations

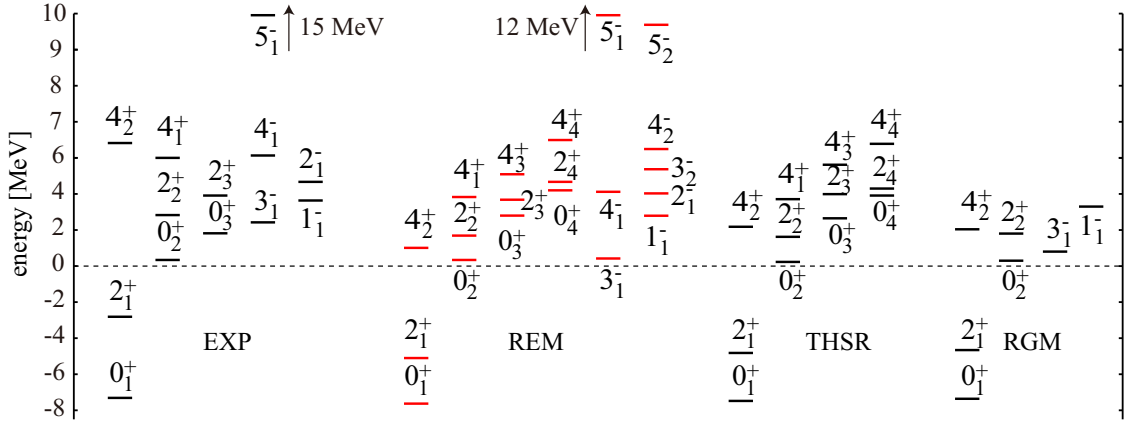


FIG. 8. (Color online) Excitation energies measured from the 3α threshold. Theoretical results by the REM, THSR [18, 23] and RGM [2, 3] are compared with the experiments [13–16, 19, 72–76]. The calculated 4_1^+ , 4_2^+ , 5_1^- and 5_2^- states are labeled accordingly the observed counterparts.

use the same Hamiltonian, and hence, they should be consistent to each other and the deeper binding energy means a better wave function for the bound states. We see that all of the theoretical results are qualitatively consistent to each other. In particular, REM and THSR results are reasonably agree for all positive-parity states which include the compact shell-model-like ground band and highly-excited cluster states. As for the negative-parity states, REM and RGM reasonably agree for the 1_1^- and 3_1^- states, and REM additionally produces the 2_1^- , 3_2^- and 4_1^- states, which are also described by AMD [5, 8] and FMD [7]. In short, REM can describe all of the states reported by THSR and RGM reasonably. It must be emphasized that not only the 0^+ states but all of the state shown in Fig. 8 were obtained from a single ensemble set 1, which means that the EOM really effectively generates the basis wave functions.

TABLE I. Calculated and observed energies measured from 3α threshold in MeV and radii in fm. Experimental data is taken from Refs. [13–16, 19, 72–76]

J^π	REM		THSR [11, 18, 23]		RGM [2, 3]		EXP	
	E	$\sqrt{\langle r^2 \rangle}$	E	$\sqrt{\langle r^2 \rangle}$	E	$\sqrt{\langle r^2 \rangle}$	E	$\sqrt{\langle r^2 \rangle}$
0_1^+	-7.6	2.4	-7.5	2.4	-7.4	2.4	-7.3	2.4
2_1^+	-5.1	2.4	-4.8	2.4	-4.6	2.4	-2.8	
4_2^+	1.0	2.3	2.2	2.3	2.0	2.3	6.8	
0_2^+	0.3	3.7	0.2	3.7	0.4	3.5	0.4	
2_2^+	1.7	3.9	1.6	3.9	2.1	4.0	2.8	
4_1^+	3.8	4.5	3.7	4.5			6.0	
0_3^+	2.8	4.6	2.7	4.7			1.8	
2_3^+	3.9	4.6	4.0	4.5			3.9	
4_3^+	5.4	4.8	5.6	4.7				
0_4^+	4.0	4.2	3.9	4.2				
2_4^+	4.6	3.7	4.3	4.1				
4_4^+	6.6	5.0	6.8	4.7				
<hr/>								
3_1^-	0.4	2.8			0.8	2.8	2.4	
4_1^-	4.1	2.9					6.1	
5_1^-	12	3.6					15	
1_1^-	2.8	4.3			3.4	3.4	3.6	
2_1^-	4.0	3.5					4.6	
3_2^-	5.4	4.5						
4_2^-	6.4	4.7						
5_2^-	9.3	4.5						

Now, we discuss the details of the energies and radii listed in Tab. I. Firstly, for many of the 2^+ and 4^+ states, we see that REM yields deeper binding energy than THSR and RGM. This may be due to the limitation of the model space of the THSR and RGM calculations. Namely, the THSR calculation assumes the axially symmetric intrinsic state and RGM calculation limits the relative angular momentum between clusters up to 2, while REM has

no such assumptions. Secondly, THSR often yields smaller excitation energies and larger radii for highly excited states such as 0_3^+ , 0_4^+ and 2_4^+ states. Although the variational principle cannot be applied to these highly excited broad resonances, the difference may be attributed to the difference in the long range part of the wave functions. THSR uses central Gaussians with large size parameters, while REM uses localized Gaussians with relatively smaller size parameters. Therefore, THSR should have better description for the long-range part of the dilute states.

We also comment the difference between the models. In the THSR calculation, the positive-parity condensate was assumed, hence the negative-parity is missing in the figure. However, if an extended version of THSR is applied, we expect that it yields the negative-parity states consistent with REM and RGM. In the RGM calculation, neither r^2 -constraint nor other techniques to eliminate the non-resonant state were applied. As a result, it cannot describe many highly excited states with large widths.

Finally, we discuss the characteristics of the excited 0^+ and 1^- states referring their electric monopole and dipole transition strengths. The transition matrix are defined as,

$$M(E0; 0_m^+ \rightarrow 0_n^+) = \langle 0_n^+ | \sum_{i=1}^A r_i'^2 \frac{1 + \tau_{zi}}{2} | 0_m^+ \rangle, \quad (27)$$

$$M(IS1; 0_m^+ \rightarrow 1_n^-) = \langle 1_n^- | \sum_{i=1}^A r_i'^3 Y_1(\hat{r}_i') | 0_m^+ \rangle, \quad (28)$$

where \mathbf{r}_i' denotes the single-particle coordinate measured from the center-of-mass. The results are summarized in Tab. II.

Since the monopole transition operator is nothing but the radius operator, the matrix element should be large for the dilute gas-like states [78]. Indeed, it is well known that the Hoyle state has the enhanced monopole transition strength from the ground state because of its dilute gas-like nature. The present calculation yields 6.4 efm^2 (1.5 WU) which is consistent with the other cluster models, but slightly overestimates the observation. The monopole transition from the ground state to the more dilute 0_3^+ state is also large and comparable with the Weisskopf unit (WU), but not as large as that of the Hoyle state. The reason of the reduction is that the 0_3^+ state is dominantly composed of the $4\hbar\omega$ configurations which cannot be excited by the monopole operator ($2\hbar\omega$ excitation). However, it must be noted that the transition from the Hoyle state to the 0_3^+ state is greatly enhanced (6.2 WU). From this result and from the analysis of the wave function, it was concluded that the 0_3^+

TABLE II. Calculated and observed electric monopole and isoscalar dipole transition matrix in the units of $e\text{fm}^2$ and fm^3 .

transition	REM	THSR [11, 18, 23]	RGM [2, 3]	EXP [77]
$0_1^+ \rightarrow 0_2^+$	6.4	6.3	6.7	5.4 ± 2
$0_1^+ \rightarrow 0_3^+$	3.8	3.9		
$0_1^+ \rightarrow 0_4^+$	3.3	3.5		
$0_2^+ \rightarrow 0_3^+$	28	34		
$0_2^+ \rightarrow 0_4^+$	0.7	0.5		
$0_1^+ \rightarrow 1_1^-$	3.7			
$0_2^+ \rightarrow 1_1^-$	45			

state is a $2\hbar\omega$ excited state built on the Hoyle state [18, 23]. In other words, it is the breathing mode of the Hoyle state [24]. This relationship between the ground, Hoyle and 0_3^+ states are schematically illustrated in Fig. 9. On the contrary, the monopole transition between the Hoyle state and the 0_4^+ state is rather weak. This is due to the structural mismatch between these states. In Ref. [23], it was concluded that the α clusters are linearly aligned in the 0_4^+ state (linear-chain state), which naturally reduces the overlap with the Hoyle state.

A new finding in the present study is that not only the 0_3^+ state but also the 1_1^- state may be an excited state of the Hoyle state. As discussed in Ref. [79], the 1_1^- states with pronounced clustering should have the strong IS dipole transition strength from the ground state. The present calculation yields $M(IS1; 0_1^+ \rightarrow 1_1^-) = 3.7 \text{ fm}^3$ which is comparable with the Weisskopf unit (0.7 WU). A similar strength was also obtained by the AMD calculation [80]. Furthermore, it must be noted that the IS dipole transition between the Hoyle state and the 1_1^- state is extraordinary strong (8.8 WU). From this result, we are tempted to conclude that the 1_1^- state is the $1\hbar\omega$ (or $3\hbar\omega$) excitation of the Hoyle state. Indeed the 1_1^- state has huge radius comparable with the 0_3^+ state. It is also interesting to note that the 1_1^- state is energetically very close to the 0_3^+ state. This conjecture is also illustrated in Fig. 9.

To discuss the similarity between the 0_3^+ and 1_1^- states in a different way, we optimized a single Brink-Bloch wave function (optimized the position of 3α clusters) so that the overlap

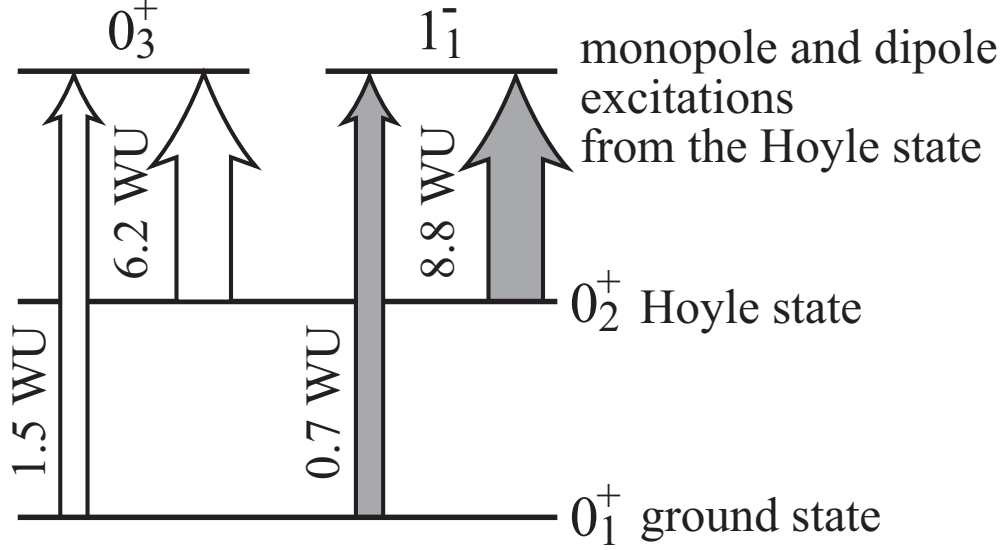


FIG. 9. Excitation modes of the Hoyle state are schematically shown. Arrows show the monopole and dipole transitions.

with the REM wave functions is maximized. Here the overlap is defined as,

$$O = \frac{|\langle \hat{P}^{J\pi} \Phi_{BB} | \Psi^{J\pi} \rangle|^2}{\langle \hat{P}^{J\pi} \Phi_{BB} | \hat{P}^{J\pi} \Phi_{BB} \rangle}, \quad (29)$$

where $\Psi^{J\pi}$ denotes the REM wave function for the 0^+ and 1^- states and Φ_{BB} is a Brink-Bloch wave function to be optimized. Thus-obtained optimized Brink-Bloch wave functions shown in Fig. 10 tell us the most likelihood cluster configuration for each state. It can be seen that the ground state is represented by a Brink-Bloch wave function with short inter-cluster distances whose overlap amounts to 0.81. This is due to the dominance of the $(0s)^4(0p)^8$ configuration which can be described by a single Brink-Bloch wave function. On the contrary, the most likelihood cluster configuration of the Hoyle state has large inter-cluster distance and it only explains about 39% of the Hoyle state. Indeed, not only the configuration shown in Fig. 10, but many other configurations also have the overlaps of the same magnitude. This indicates that the Hoyle state is not a single cluster configuration but a superposition of many different configurations, which is consistent with the dilute nature of the Hoyle state. The dilute character can be more strongly seen in the 0_3^+ and 1_1^- states. The likelihood configurations of these states have the inter-cluster distances larger than the Hoyle state, and the overlaps are rather small. Thus, we expect that the 1_1^- state

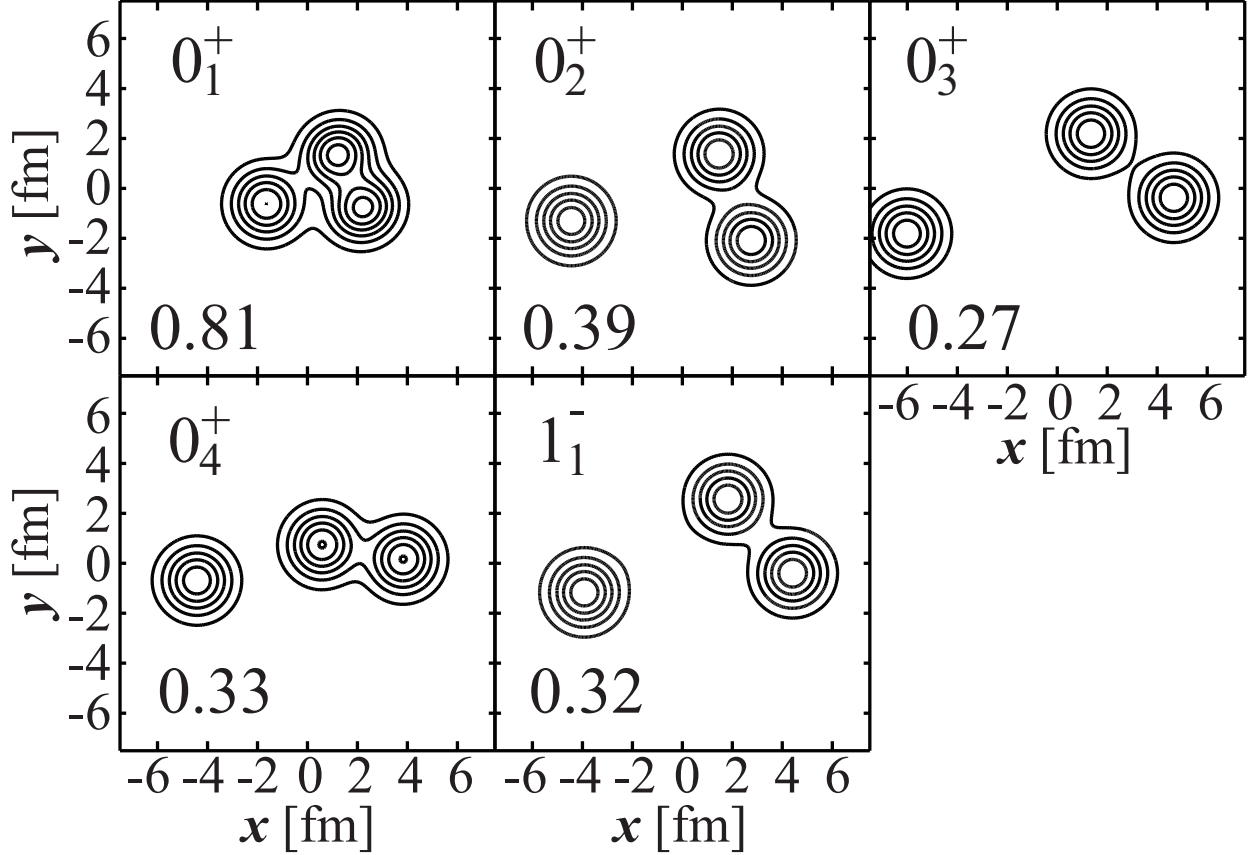


FIG. 10. The most liklihood cluster configurations for the 0^+ and 1^- states. Numbers in the panels show the maximum overlap defined by Eq. (29).

can be also regarded as the family of the Hoyle state. We also comment that the 0_4^+ state does not look a perfect linear-chain configuration, but has a bent-armed configuration. The smallness of the overlap may mean that this state is not stable against the bending motion. This interpretation is consistent with the discussion made in Refs. [8, 23, 42]. We also note that this cluster configuration is more or less similar to the bent-armed cluster configuration of the Hoyle state suggested by the Lattice calculation [81].

IV. SUMMARY

In summary, we have developed a new theoretical model which utilizes the classical EOM of the Gaussian centroids to generate the ergodic ensemble of the basis wave functions. The generated basis wave functions are superposed to diagonalize the Hamiltonian. Thus, the

method named REM can be regarded a generator coordinate method which employs the real time t as the generator coordinate.

As a benchmark of REM, we applied it to the 3α system (^{12}C) and found that the result is consistent with or even better than the other cluster models. It was shown that when the propagation time is long enough the energies and radii of the ground and many excited states are converged and independent of the initial condition. As a result, REM successfully described all of the states reported by THSR and RGM. It must be emphasized that all the states are obtained from a single ensemble of the basis wave function, which indicates that the EOM effectively generates the basis wave functions. However, even if we apply the r^2 -constraint, several excited states were not converged well because of the contamination of the non-resonant wave function. Particular case is the 0_3^+ state which has broad width and is regarded as the breathing mode of the Hoyle state. More accurate description of these states requires further development of the method.

Based on the isoscalar monopole and dipole transition strengths, the characteristics of the excited 0^+ and 1^- states are discussed. We confirmed that the properties of the Hoyle state and the 0_3^+ states are consistent with those discussed in the preceding studies. They have dilute structure and the enhanced monopole transition strengths from the ground state. The huge monopole transition strength between the Hoyle state and the 0_3^+ state was also confirmed. In addition to this, we found that the 1_1^- state has the analogous properties to the 0_3^+ state. Namely, the 1_1^- state has dilute structure and the enhanced dipole transition strengths from the ground state. It also has the extraordinary large IS dipole strength from the Hoyle state. From these results, we conjecture that the 1_1^- state can be also regarded as an excitation mode of the Hoyle state. Although this conjecture is based on only the transition strengths and the overlaps, more detailed quantitative discussion based on the reduced width amplitudes, transition form factors and occupation probabilities will be made in our forthcoming papers.

ACKNOWLEDGMENTS

The authors acknowledge that this work was initiated by the discussion with Dr. Kanada-En'yo and Dr. Yabana. They also acknowledge the fruitful discussions with Dr. Zhou, Dr. Funaki, Dr. Horiuchi and Dr. Kawabata. This work was supported by JSPS KAKENHI

- [1] E. Uegaki, Y. Abe, S. Okabe, and H. Tanaka, Prog. Theor. Phys. **59**, 1031 (1978).
- [2] Y. Fujiwara, H. Horiuchi, K. Ikeda, M. Kamimura, K. Kato, Y. Suzuki, and E. Uegaki, Prog. Theor. Phys. Suppl. **68**, 29 (1980).
- [3] M. Kamimura, Nucl. Phys. A **351**, 456 (1981).
- [4] P. Descouvemont and D. Baye, Phys. Rev. C **36**, 54 (1987).
- [5] Y. Kanada-En'yo, Phys. Rev. Lett. **81**, 5291 (1998).
- [6] P. Descouvemont, C. Daniel, and D. Baye, Phys. Rev. C **67**, 044309 (2003).
- [7] M. Chernykh, H. Feldmeier, T. Neff, P. von Neumann-Cosel, and A. Richter, Phys. Rev. Lett. **98**, 032501 (2007).
- [8] Y. Kanada-En'yo, Prog. Theor. Phys. **117**, 655 (2007).
- [9] A. Tohsaki, H. Horiuchi, P. Schuck, and G. Röpke, Phys. Rev. Lett. **87**, 192501 (2001).
- [10] T. Yamada, Y. Funaki, H. Horiuchi, G. Röpke, P. Schuck, and A. Tohsaki, in *Lect. Notes Phys. Clust. Nuclei, Vol.2*, edited by C. Beck (Springer, Berlin, Heidelberg, 2012) Chap. 5, pp. 229–298.
- [11] P. Schuck, Y. Funaki, H. Horiuchi, G. Röpke, A. Tohsaki, and T. Yamada, Phys. Scr. **91**, 123001 (2016).
- [12] M. Freer, H. Fujita, Z. Buthelezi, J. Carter, R. W. Fearick, S. V. Förtsch, R. Neveling, S. M. Perez, P. Papka, F. D. Smit, J. A. Swartz, and I. Usman, Phys. Rev. C **80**, 041303 (2009).
- [13] M. Itoh, H. Akimune, M. Fujiwara, U. Garg, N. Hashimoto, T. Kawabata, K. Kawase, S. Kishi, T. Murakami, K. Nakanishi, Y. Nakatsugawa, B. K. Nayak, S. Okumura, H. Sakaguchi, H. Takeda, S. Terashima, M. Uchida, Y. Yasuda, M. Yosoi, and J. Zenihiro, Phys. Rev. C **84**, 054308 (2011).
- [14] W. R. Zimmerman, N. E. Destefano, M. Freer, M. Gai, and F. D. Smit, Phys. Rev. C **84**, 027304 (2011).
- [15] W. R. Zimmerman, M. W. Ahmed, B. Bromberger, S. C. Stave, A. Breskin, V. Dangendorf, T. Delbar, M. Gai, S. S. Henshaw, J. M. Mueller, C. Sun, K. Tittelmeier, H. R. Weller, and Y. K. Wu, Phys. Rev. Lett. **110**, 152502 (2013).
- [16] M. Freer, S. Almaraz-Calderon, A. Aprahamian, N. I. Ashwood, M. Barr, B. Bucher, P. Copp,

- M. Couder, N. Curtis, X. Fang, F. Jung, S. Leshner, W. Lu, J. D. Malcolm, A. Roberts, W. P. Tan, C. Wheldon, and V. A. Ziman, Phys. Rev. C **83**, 034314 (2011).
- [17] M. Freer and H. Fynbo, Prog. Part. Nucl. Phys. **78**, 1 (2014).
- [18] Y. Funaki, Phys. Rev. C **92**, 021302 (2015).
- [19] M. Itoh, H. Akimune, M. Fujiwara, U. Garg, T. Kawabata, K. Kawase, T. Murakami, K. Nakanishi, Y. Nakatsugawa, H. Sakaguchi, S. Terashima, M. Uchida, Y. Yasuda, M. Yosoi, and J. Zenihiro, J. Phys. Conf. Ser. **436**, 012006 (2013).
- [20] C. Kurokawa and K. Kato, Phys. Rev. C **71**, 021301 (2005).
- [21] C. Kurokawa and K. Kato, Nucl. Phys. A **792**, 87 (2007).
- [22] S.-I. Ohtsubo, Y. Fukushima, M. Kamimura, and E. Hiyama, Prog. Theor. Exp. Phys. **2013** (2013).
- [23] Y. Funaki, Phys. Rev. C **94**, 024344 (2016).
- [24] B. Zhou, A. Tohsaki, H. Horiuchi, and Z. Ren, Phys. Rev. C **94**, 044319 (2016).
- [25] T. Wakasa, E. Ihara, K. Fujita, Y. Funaki, K. Hatanaka, H. Horiuchi, M. Itoh, J. Kamiya, G. Röpke, H. Sakaguchi, N. Sakamoto, Y. Sakemi, P. Schuck, Y. Shimizu, M. Takashina, S. Terashima, A. Tohsaki, M. Uchida, H. Yoshida, and M. Yosoi, Phys. Lett. B **653**, 173 (2007).
- [26] Y. Funaki, T. Yamada, H. Horiuchi, G. Röpke, P. Schuck, and A. Tohsaki, Phys. Rev. Lett. **101**, 082502 (2008).
- [27] N. Curtis, S. Almaraz-Calderon, A. Aprahamian, N. I. Ashwood, M. Barr, B. Bucher, P. Copp, M. Couder, X. Fang, M. Freer, G. Goldring, F. Jung, S. R. Leshner, W. Lu, J. D. Malcolm, A. Roberts, W. P. Tan, C. Wheldon, and V. A. Ziman, Phys. Rev. C **88**, 064309 (2013).
- [28] M. R. D. Rodrigues, T. Borello-Lewin, H. Miyake, J. L. M. Duarte, C. L. Rodrigues, M. A. Souza, L. B. Horodyski-Matsushigue, G. M. Ukita, F. Cappuzzello, A. Cunsolo, M. Cavallaro, C. Agodi, and A. Foti, Phys. Rev. C **89**, 024306 (2014).
- [29] R. Bijker and F. Iachello, Phys. Rev. Lett. **112**, 152501 (2014).
- [30] A. A. Ogloblin, A. N. Danilov, A. S. Demyanova, S. A. Goncharov, and T. L. Belyaeva, Phys. Rev. C **94**, 051602 (2016).
- [31] R. Bijker and F. Iachello, Nucl. Phys. A **957**, 154 (2017).
- [32] K. C. W. Li, R. Neveling, P. Adsley, P. Papka, F. D. Smit, J. W. Brümmer, C. A. Diget, M. Freer, M. N. Harakeh, T. Kokalova, F. Nemulodi, L. Pellegri, B. Rebeiro, J. A. Swartz,

- S. Triambak, J. J. van Zyl, and C. Wheldon, Phys. Rev. C **95**, 031302 (2017).
- [33] T. Yamada and P. Schuck, Phys. Rev. C **69**, 024309 (2004).
 - [34] T. Kokalova, N. Itagaki, W. von Oertzen, and C. Wheldon, Phys. Rev. Lett. **96**, 192502 (2006).
 - [35] N. Itagaki, M. Kimura, C. Kurokawa, M. Ito, and W. von Oertzen, Phys. Rev. C **75**, 037303 (2007).
 - [36] P. Descouvemont, Nucl. Phys. A **584**, 532 (1995).
 - [37] Y. Kanada-En'yo, Phys. Rev. C **75**, 024302 (2007).
 - [38] T. Kawabata, H. Akimune, H. Fujita, Y. Fujita, M. Fujiwara, K. Hara, K. Hatanaka, M. Itoh, Y. Kanada-En'yo, S. Kishi, K. Nakanishi, H. Sakaguchi, Y. Shimbara, A. Tamii, S. Terashima, M. Uchida, T. Wakasa, Y. Yasuda, H. Yoshida, and M. Yosoi, Phys. Lett. B **646**, 6 (2007).
 - [39] T. Yamada and Y. Funaki, Phys. Rev. C **82**, 064315 (2010).
 - [40] T. Yamada, H. Horiuchi, and P. Schuck, Mod. Phys. Lett. A **21**, 2373 (2006).
 - [41] T. Yamada and Y. Funaki, Phys. Rev. C **92**, 034326 (2015).
 - [42] N. Itagaki, S. Okabe, K. Ikeda, and I. Tanihata, Phys. Rev. C **64**, 014301 (2001).
 - [43] T. Suhara and Y. Kanada-En'yo, Phys. Rev. C **82**, 044301 (2010).
 - [44] M. Freer, J. D. Malcolm, N. L. Achouri, N. I. Ashwood, D. W. Bardayan, S. M. Brown, W. N. Catford, K. A. Chipps, J. Cizewski, N. Curtis, K. L. Jones, T. Munoz-Britton, S. D. Pain, N. Soić, C. Wheldon, G. L. Wilson, and V. A. Ziman, Phys. Rev. C **90**, 054324 (2014).
 - [45] T. Baba, Y. Chiba, and M. Kimura, Phys. Rev. C **90**, 064319 (2014).
 - [46] J.-P. Ebran, E. Khan, T. Nikšić, and D. Vretenar, Phys. Rev. C **90**, 054329 (2014).
 - [47] D. Dell'Aquila, I. Lombardo, L. Acosta, R. Andolina, L. Auditore, G. Cardella, M. B. Chatterjee, E. De Filippo, L. Francalanza, B. Gnofo, G. Lanzalone, A. Pagano, E. V. Pagano, M. Papa, S. Pirrone, G. Politi, F. Porto, L. Quattrocchi, F. Rizzo, E. Rosato, P. Russotto, A. Trifirò, M. Trimarchi, G. Verde, and M. Vigilante, Phys. Rev. C **93**, 024611 (2016).
 - [48] A. Fritsch, S. Beceiro-Novo, D. Suzuki, W. Mittig, J. J. Kolata, T. Ahn, D. Bazin, F. D. Becchetti, B. Bucher, Z. Chajecki, X. Fang, M. Febraro, A. M. Howard, Y. Kanada-En'yo, W. G. Lynch, A. J. Mitchell, M. Ojaruega, A. M. Rogers, A. Shore, T. Suhara, X. D. Tang, R. Torres-Isea, and H. Wang, Phys. Rev. C **93**, 014321 (2016).
 - [49] Z. Y. Tian, Y. L. Ye, Z. H. Li, C. J. Lin, Q. T. Li, Y. C. Ge, J. L. Lou, W. Jiang, J. Li, Z. H. Yang, J. Feng, P. J. Li, J. Chen, Q. Liu, H. L. Zang, B. Yang, Y. Zhang, Z. Q. Chen, Y. Liu,

- X. H. Sun, J. Ma, H. M. Jia, X. X. Xu, L. Yang, N. R. Ma, and L. J. Sun, Chinese Phys. C **40**, 111001 (2016).
- [50] T. Baba and M. Kimura, Phys. Rev. C **94**, 044303 (2016).
- [51] J. Li, Y. L. Ye, Z. H. Li, C. J. Lin, Q. T. Li, Y. C. Ge, J. L. Lou, Z. Y. Tian, W. Jiang, Z. H. Yang, J. Feng, P. J. Li, J. Chen, Q. Liu, H. L. Zang, B. Yang, Y. Zhang, Z. Q. Chen, Y. Liu, X. H. Sun, J. Ma, H. M. Jia, X. X. Xu, L. Yang, N. R. Ma, and L. J. Sun, Phys. Rev. C **95**, 021303 (2017).
- [52] H. Yamaguchi, D. Kahl, S. Hayakawa, Y. Sakaguchi, K. Abe, T. Nakao, T. Suhara, N. Iwasa, A. Kim, D. Kim, S. Cha, M. Kwag, J. Lee, E. Lee, K. Chae, Y. Wakabayashi, N. Imai, N. Kitamura, P. Lee, J. Moon, K. Lee, C. Akers, H. Jung, N. Duy, L. Khiem, and C. Lee, Phys. Lett. B **766**, 11 (2017).
- [53] T. Baba and M. Kimura, (2017), arXiv:1702.04874.
- [54] D. L. Hill and J. A. Wheeler, Phys. Rev. **89**, 1102 (1953).
- [55] J. J. Griffin and J. A. Wheeler, Phys. Rev. **108**, 311 (1957).
- [56] Y. Suzuki and K. Varga, in *Stoch. Var. Approach to Quantum-Mechanical Few-Body Probl.* (Springer Berlin Heidelberg, Berlin, Heidelberg, 1998).
- [57] N. Itagaki, A. Kobayakawa, and S. Aoyama, Phys. Rev. C **68**, 054302 (2003).
- [58] J. Mitroy, S. Bubin, W. Horiuchi, Y. Suzuki, L. Adamowicz, W. Cencek, K. Szalewicz, J. Komasa, D. Blume, and K. Varga, Rev. Mod. Phys. **85**, 693 (2013).
- [59] Y. Fukuoka, S. Shinohara, Y. Funaki, T. Nakatsukasa, and K. Yabana, Phys. Rev. C **88**, 014321 (2013).
- [60] D. M. Brink, *Proc. Int. School of Physics Enrico Fermi, Course 36, Varenna*, edited by C. Bloch (Academic Press, New York, 1966).
- [61] Y. Funaki, A. Tohsaki, H. Horiuchi, P. Schuck, and G. Röpke, Phys. Rev. C **67**, 051306 (2003).
- [62] M. Saraceno, P. Kramer, and F. Fernandez, Nucl. Phys. A **405**, 88 (1983).
- [63] J. Schnack and H. Feldmeier, Nucl. Phys. A **601**, 181 (1996).
- [64] A. Ono and H. Horiuchi, Phys. Rev. C **53**, 2341 (1996).
- [65] A. Ono and H. Horiuchi, Phys. Rev. C **53**, 845 (1996).
- [66] J. Schnack and H. Feldmeier, Phys. Lett. B **409**, 6 (1997).
- [67] Y. Sugawa and H. Horiuchi, Phys. Rev. C **60**, 064607 (1999).

- [68] T. Furuta and A. Ono, Phys. Rev. C **74**, 014612 (2006).
- [69] Y. Kanada-En'yo, M. Kimura, and A. Ono, Prog. Theor. Exp. Phys. **2012**, 1A202 (2012).
- [70] A. Volkov, Nucl. Phys. **74**, 33 (1965).
- [71] Y. Funaki, H. Horiuchi, and A. Tohsaki, Prog. Theor. Phys. **115**, 115 (2006).
- [72] F. Ajzenberg-Selove, Nucl. Phys. A **506**, 1 (1990).
- [73] M. Freer, I. Boztosun, C. A. Bremner, S. P. G. Chappell, R. L. Cowin, G. K. Dillon, B. R. Fulton, B. J. Greenhalgh, T. Munoz-Britton, M. P. Nicoli, W. D. M. Rae, S. M. Singer, N. Sparks, D. L. Watson, and D. C. Weissner, Phys. Rev. C **76**, 034320 (2007).
- [74] O. S. Kirsebom, M. Alcorta, M. J. G. Borge, M. Cubero, C. A. Diget, R. Dominguez-Reyes, L. M. Fraile, B. R. Fulton, H. O. U. Fynbo, S. Hyldegaard, B. Jonson, M. Madurga, A. Muñoz Martin, T. Nilsson, G. Nyman, A. Perea, K. Riisager, and O. Tengblad, Phys. Rev. C **81**, 064313 (2010).
- [75] M. Freer, M. Itoh, T. Kawabata, H. Fujita, H. Akimune, Z. Buthelezi, J. Carter, R. W. Fearick, S. V. Försch, M. Fujiwara, U. Garg, N. Hashimoto, K. Kawase, S. Kishi, T. Murakami, K. Nakanishi, Y. Nakatsugawa, B. K. Nayak, R. Neveling, S. Okumura, S. M. Perez, P. Papka, H. Sakaguchi, Y. Sasamoto, F. D. Smit, J. A. Swartz, H. Takeda, S. Terashima, M. Uchida, I. Usman, Y. Yasuda, M. Yosoi, and J. Zenihiro, Phys. Rev. C **86**, 034320 (2012).
- [76] D. J. Marín-Lámbbari, R. Bijker, M. Freer, M. Gai, T. Kokalova, D. J. Parker, and C. Wheldon, Phys. Rev. Lett. **113**, 012502 (2014).
- [77] P. Strehl, Zeitschrift für Phys. A Hadron. Nucl. **234**, 416 (1970).
- [78] T. Yamada, Y. Funaki, H. Horiuchi, K. Ikeda, and A. Tohsaki, Prog. Theor. Phys. **120**, 1139 (2008).
- [79] Y. Chiba, M. Kimura, and Y. Taniguchi, Phys. Rev. C **93**, 034319 (2016).
- [80] Y. Kanada-En'yo, Phys. Rev. C **93**, 054307 (2016).
- [81] E. Epelbaum, H. Krebs, T. A. Lähde, D. Lee, and U.-G. Meißner, Phys. Rev. Lett. **109**, 252501 (2012).